

Article

Dissolution of Magnesia in Silicate Melts and Diffusivity Determination from CLSM Studies

Burhanuddin *  and Harald Harmuth

Chair of Ceramics, Montanuniversitaet Leoben, Peter-Tunner Straße 5, 8700 Leoben, Austria

* Correspondence: burhanuddin.burhanuddin@unileoben.ac.at; Tel.: +43-384-2402-3217; Fax: +43-384-2402-3202

Abstract: Magnesia is one of the vital and extensively used refractory components. In this study, the dissolution of magnesia is investigated at 1450, 1500, and 1550 °C in three silicate slags in the CaO–Al₂O₃–SiO₂–MgO system using high-temperature confocal laser scanning microscopy to determine its effective binary diffusivity. The pore-free fragments of single-crystal fused magnesia particles were used, and the effects of experimental parameters and slag properties on the dissolution of magnesia were assessed. The ranking of dissolution times in the three slags at the three temperatures did not agree with the trend expected from the CaO/SiO₂ ratio of each slag. Instead, several quotients serving as reference numbers were tested. The effective binary diffusivities were calculated considering all the impacting phenomena and parameters. The diffusivities of magnesia at 1500 °C in the slags with CaO/SiO₂ weight ratios of 0.65, 0.93, and 1.17 are 2.67×10^{-10} , 1.81×10^{-10} , and 3.20×10^{-10} m²/s, respectively. The diffusivity of magnesia in one of the three slags was compared with rotating finger test results, which showed good agreement. The plausibility of diffusivity was checked using an Arrhenius plot.

Keywords: magnesia; corrosion resistance; diffusivity; dissolution



Citation: Burhanuddin; Harmuth, H. Dissolution of Magnesia in Silicate Melts and Diffusivity Determination from CLSM Studies. *Appl. Sci.* **2023**, *13*, 8458. <https://doi.org/10.3390/app13148458>

Academic Editor: Leonid Burakovsky

Received: 12 June 2023

Revised: 18 July 2023

Accepted: 20 July 2023

Published: 21 July 2023



Copyright: © 2023 by the authors. Licensee MDPI, Basel, Switzerland. This article is an open access article distributed under the terms and conditions of the Creative Commons Attribution (CC BY) license (<https://creativecommons.org/licenses/by/4.0/>).

1. Introduction

Magnesia is one of the widely used refractory components in pyro-metallurgy and cement industries [1–5]. When applied to a working lining, it is susceptible to corrosion owing to the corrosive charge at elevated temperatures, including dissolution in melts. Refractory corrosion often seriously hampers the production performance of vessels and the product quality [6].

To design a resource- and cost-efficient refractory with a longer service life, the dissolution of the refractory component must be studied thoroughly in different corrosive melts [7,8]. Diffusivity is the primary parameter used to quantify dissolution [2,7,9–11]. The diffusivities of the dissolving species can be experimentally determined. In the last two and half decades, high-temperature confocal laser scanning microscopy (HT-CLSM) has become a popular tool for dissolution studies [9,10,12–25]. The in situ measurements and possibility of maintaining a high slag-to-particle mass ratio make this method important for dissolution studies. However, only small particles can be studied using this apparatus. In several reported CLSM dissolution studies [9,10,12–23], all of the influencing phenomena and parameters, particularly the effects of slag bath motion and Stefan flow, were not incorporated into the evaluation methods. Ogris and Gamsjaeger [26] accounted for Stefan flow, but the effect of bath motion was not considered. However, both of the phenomena were incorporated in Ref. [11]. The main hurdle in determining the diffusivity from CLSM studies is the appropriate depiction of the effective diffusive boundary layer thickness. In Ref. [11], a method for appropriately depicting the effective diffusive boundary layer thickness by integrating the effect of bath motion and related flow parameters using the Sherwood relation is described in detail. The same method for determining the diffusivity was employed in this study.

Few dissolution studies on magnesia using HT-CLSM and their diffusivities are available in the literature [10,16,21,23]. In these studies, the effects of slag bath motion and Stefan flow on diffusivity determination were not considered. However, the effect of slag basicity on magnesia dissolution has not been extensively studied. In the present study, the dissolution of magnesia particles in three silicate slags at 1450, 1500, and 1550 °C have been studied to enrich the literature with effective binary diffusivities of magnesia determined with the consideration of all influencing phenomena and parameters. Furthermore, we tried to establish a parameter for the qualitative estimation of dissolution, which is not possible with slag basicity only. The aforesaid parameter consisted of the dimensionless concentration difference (B), thermodynamic factor (f), effective diffusive boundary layer thickness (δ), and slag viscosity (η). Additionally, the diffusivities of magnesia in one of these three slags were weighed against the findings obtained from dynamic finger test experiments [8] where the δ could be accurately controlled.

2. Materials and Methods

2.1. Materials

In this study, pore-free fragments of single-crystal fused magnesia particles close to the theoretical density of 3.58 g/cc, with a magnesia content of 98.66 wt% and sizes of 300–500 μm , were investigated in three silicate slags. In this study, fused magnesia grains were used because dense spherical magnesia particles are not commercially available. Cubic-shaped particles were manually selected, which transformed into a spherical shape at the beginning of the experiment owing to the faster dissolution of the edges. Synthetic slags in the CaO–Al₂O₃–SiO₂–MgO system were produced from quartz powder, calcined Al₂O₃ powder, decarburized CaCO₃, and MgO powder (S3 Handel und Dienstleistungen UG, Bad Oeynhausen, Germany). The slag preparation procedure was adopted from Ref. [11]. Each of the raw materials was taken as per the target slag composition and mixed to prepare slag batches. To enhance the homogeneity, the pre-mixes were melted at 1450 °C for 15 min in a preheated furnace and quenched on a metal sheet. To enhance the uniformity and maintain the same slag quantity in all CLSM crucibles, the solidified slag was pulverized in a cup mill lined with tungsten carbide. In two steps (0.08 g + 0.12 g), the powdered slag was pre-molten in each platinum-10% Rhodium (Pt-Rh10) crucible at 1450 °C for 15 min in a preheated furnace for easy removal of bubbles, which are detrimental in CLSM dissolution experiments [11]. The chemical compositions, dynamic viscosities (η) at the three experimental temperatures, and liquidus temperatures (T_L) are listed in Table 1, where C/S is the CaO/SiO₂ weight ratio. Table 2 represents the densities (ρ) of the slags and mass fractions of magnesia (w_s) in the saturated slags at 1450, 1500, and 1550 °C. The viscosities and thermochemical properties of the slags were calculated using FactSage[®] 7.3. The slag densities were determined according to the method reported in Ref. [27].

Table 1. Chemical compositions, viscosities, and liquidus temperatures of the slags.

Slag No.	C/S	CaO [wt%]	Al ₂ O ₃ [wt%]	SiO ₂ [wt%]	MgO [wt%]	$\eta_{1450^\circ\text{C}}$ [Pa·s]	$\eta_{1500^\circ\text{C}}$ [Pa·s]	$\eta_{1550^\circ\text{C}}$ [Pa·s]	T_L [°C]
S1	0.65	32.42	11.16	49.56	6.86	1.02	0.73	0.53	1265
S2	0.93	38.07	21.00	40.93	-	1.28	0.88	0.62	1301
S3	1.17	45.03	11.33	38.64	5.00	0.36	0.27	0.20	1317

Table 2. Slag densities and mass fractions of magnesia in the saturated slags.

Slag No.	$\rho_{1450^\circ\text{C}}$ [kg/m ³]	$\rho_{1500^\circ\text{C}}$ [kg/m ³]	$\rho_{1550^\circ\text{C}}$ [kg/m ³]	$W_{s,1450^\circ\text{C}}$ []	$W_{s,1500^\circ\text{C}}$ []	$W_{s,1550^\circ\text{C}}$ []
S1	2595	2587	2579	0.2724	0.2749	0.2779
S2	2611	2600	2589	0.1881	0.1932	0.1987
S3	2671	2662	2653	0.1551	0.1592	0.1637

2.2. Experimental

In this study, the dissolution of magnesia at 1450, 1500, and 1550 °C under air atmosphere was investigated using HT-CLSM at Montanuniversitaet, Leoben. Refs. [28,29] provide a complete description of the device used; the experimental procedure reported in Ref. [11] was used. The measured furnace temperature may differ from the slag temperature because the furnace thermocouple is situated a few millimeters below the slag-filled crucible. Before starting the dissolution experiments, the temperature difference between the furnace and slag was measured using an S-type thermocouple inserted into the pre-molten slag. The temperature difference was incorporated into the furnace heating program to achieve the target slag temperature. At around 20 °C, a magnesia particle was placed in the middle of a slag-filled Pt-Rh10 crucible. Thereafter, the heating schedule of the mirror furnace was started, where the heating rate was 50 °C/min until 150 °C. After 1 min of dwell time at this temperature, the heating rate was set to 500 °C/min until 50 °C below the target temperature and then reduced to 100 °C/min to achieve the target temperature. Near the target temperature, the heating program was kept on hold. The temperature was manually controlled to avoid overheating and uphold the target temperature until the complete dissolution of the particle. Subsequently, the cooling rate was set to 400 °C/min [11]. Video was captured from 150 °C until the dissolution process at the target temperature was complete. Five experiments (only four experiments at 1550 °C in S1) were carried out at each experimental temperature to confirm the repeatability and obtain representative results.

2.3. Analysis

The image analyzing software ImageJ 1.52a was used to analyze the videos at the isothermal target temperatures for each individual dissolution experiment until complete dissolution. The areas of the particle images at different frames were measured and utilized to determine the equivalent particle diameters (\varnothing) at the corresponding dissolution times. The time interval for the video analysis was adjusted according to the total dissolution time to obtain at least 30 data points. As an example, Figure 1 shows snapshots of two different time frames from the CLSM video of magnesia dissolution in S3 at 1450 °C. Upon reaching the isothermal target temperature in all experiments, the equivalent diameters were usually different. Therefore, 300 μm was selected as the initial equivalent diameter for a better comparison.

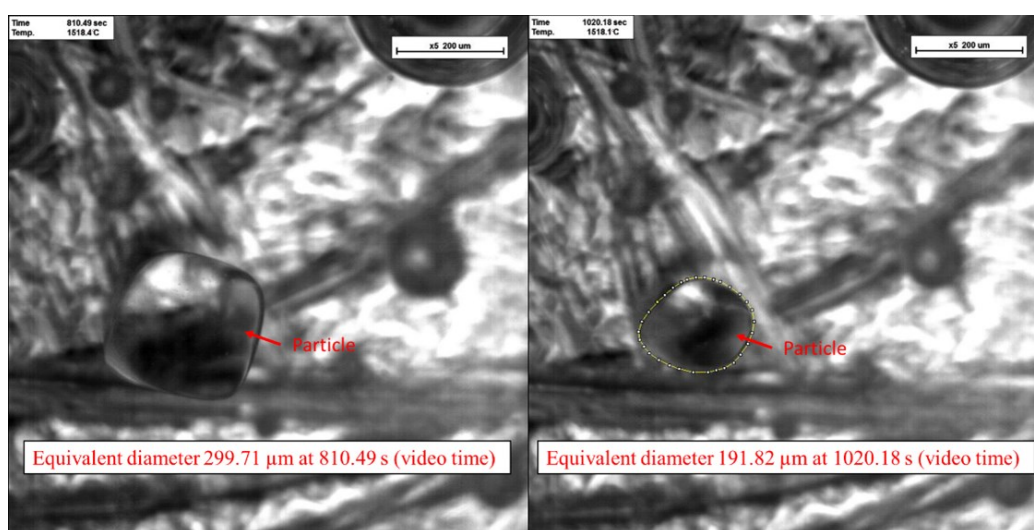


Figure 1. Snapshots of two different time frames from the CLSM video of magnesia dissolution in S3 at 1450 °C. The equivalent diameter was calculated considering a sphere of the same surface area as the measured particle.

3. Results and Discussion

3.1. Dissolution

Figure 2a–c show the dissolution curves of equivalent diameters over time in S1, S2, and S3 at 1450, 1500, and 1550 °C, respectively. The shaded area represents the standard deviation of dissolution time for a particular equivalent diameter in the corresponding experiments. Figure 2d shows the reciprocal of total dissolution time, t_{tot} (mean of the corresponding experiments), for a 300 μm particle at three temperatures in S1, S2, and S3. In all cases, time for the complete dissolution of a 300 μm particle decreases with rising experimental temperature. This is expected because of the increase in diffusivity with temperature, and it agrees with the trend of decreasing slag viscosity with increasing temperature, as shown in Table 1. In the case of magnesia, a dissolution time increase is expected with an increasing C/S ratio. However, at 1450 and 1500 °C, the sequences of S2 and S3 contradict this expectation.

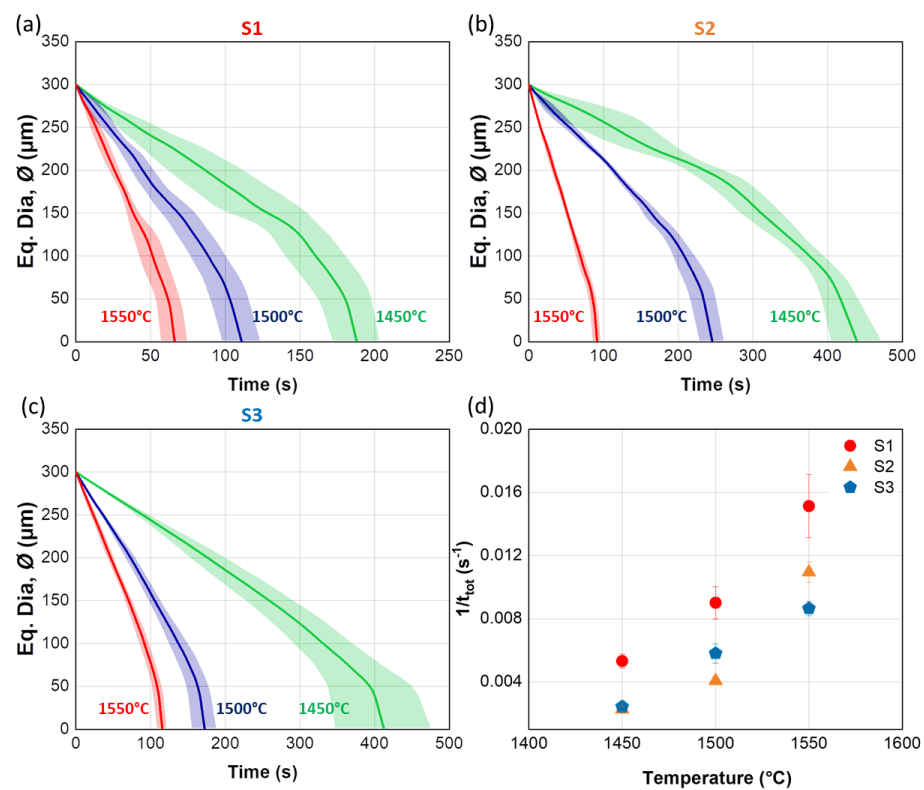


Figure 2. Dissolution curves for magnesia in (a) S1, (b) S2, and (c) S3 at 1450, 1500, and 1550 °C; (d) reciprocal of total dissolution times; shaded area represents the standard deviation of dissolution time.

Figure 3a–c show the dissolution rates in terms of the derivative of particle size $d\phi/dt$ with respect to time in S1, S2, and S3 at 1450, 1500, and 1550 °C, respectively. In all slags, at a particular temperature, the absolute value of the dissolution rate decreases to a minimum at the beginning owing to the development of a quasi-steady diffusive boundary layer; it then increases because the quasi-steady diffusive boundary layer thickness decreases in accordance with the particle radius. Similar to the total dissolution time, the absolute value of the dissolution rate increases with rising temperature; however, it does not show the expected trend with an increasing C/S ratio. Here, the concentration difference in magnesia between the saturated and bulk slag decreases with an increasing C/S ratio; this parameter acts to decrease the dissolution rate with a rising C/S ratio, but other factors also play important roles. Dissolution is inversely proportional to the δ , which is influenced by the fluid flow field around the dissolving particle and slag viscosity. According to the process in Ref. [11], average effective diffusive boundary layer thicknesses were determined from

the experimental mean dissolution curves, presented in Figure 3d. Based on the aforesaid factors, we consider introducing two parameters, B/η and $B/(\eta \cdot \delta)$, to assess the dissolution trend. The dimensionless concentration difference B is defined by Equation (1).

$$B = \frac{w_s - w_0}{1 - w_s}, \tag{1}$$

where w_0 and w_s are the mass fractions of magnesia in bulk and saturated slags, respectively. However, these parameters do not explain the dissolution trend of magnesia in the three slags. For further improvement, the thermodynamic factor of diffusion f , defined by Equation (2), was calculated using the magnesia activity coefficient (γ) calculated from the FactSage[®] results.

$$f = 1 + \frac{d \ln \gamma}{d \ln x} \tag{2}$$

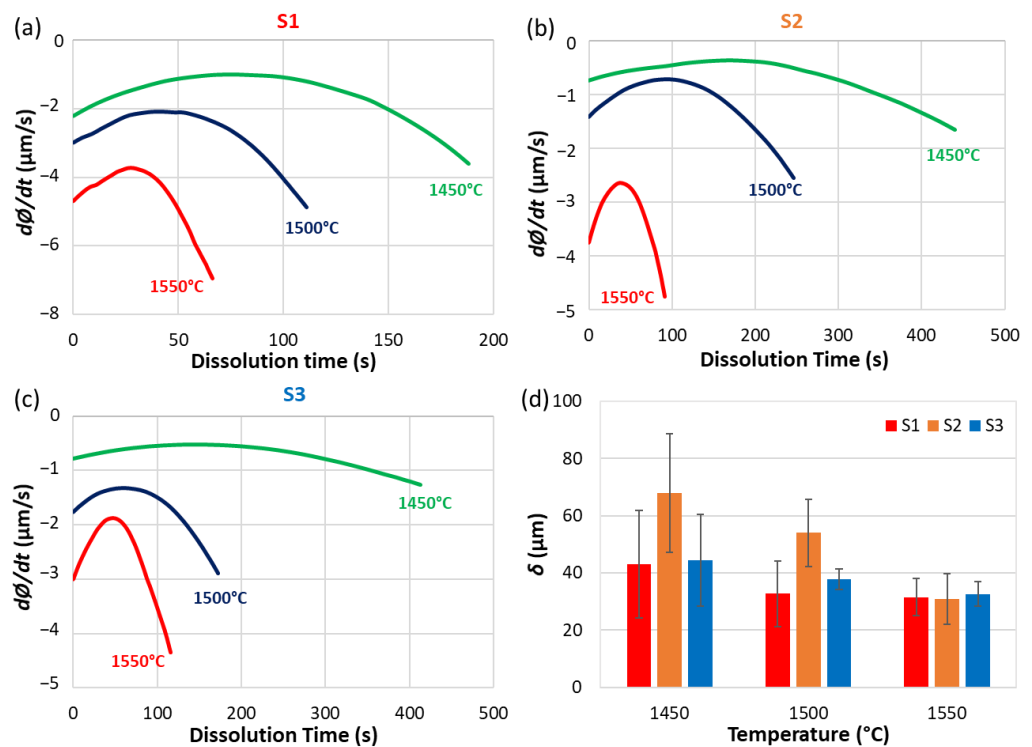


Figure 3. Dissolution rates for magnesia in (a) S1, (b) S2, and (c) S3 at 1450, 1500, and 1550 °C; (d) effective boundary layer thicknesses (δ) in S1, S2, and S3 at 1450, 1500, and 1550 °C.

The extended parameter $B \cdot f / (\eta \cdot \delta)$ was introduced, and it successfully explains the dissolution trend at 1450 and 1500 °C. For 1550 °C, it identifies the most corrosive slag as S1; the ratios B/η and $B/(\eta \cdot \delta)$ do not successfully quantify this improvement. Notably, $B \cdot D / \delta$ gives the correct ranking of dissolution times for all slags and temperatures, although the ratio f/η is not sufficiently proportional to diffusivity. This deficiency in the simplified assessment can be observed for 1550 °C rather than for the other two cases, which follows the form of the lower variance in dissolution times for slag S3. The coefficients of variation for the dissolution times of S1 and S2 are 39.8% and 38.2%, respectively, but only 27.2% for S3. Table 3 represents the dissolution parameters which can be used to assess the aggressiveness of the slag for magnesia dissolution.

Table 3. Dissolution parameters to rank the slag aggressiveness.

Temperature (°C)	Slag	t_{tot} (s)	B/η (1/Pa·s)	$B/(\eta \cdot \delta) \cdot (1/\text{Pa} \cdot \text{s} \cdot \text{m})$	$B \cdot f/(\eta \cdot \delta) \cdot (1/\text{Pa} \cdot \text{s} \cdot \text{m})$
1450	S1	188.1	0.275	6.38×10^3	2.84×10^4
	S2	439.5	0.181	2.67×10^3	8.18×10^3
	S3	412.6	0.346	7.79×10^3	2.25×10^4
1500	S1	111	0.390	1.19×10^4	5.35×10^4
	S2	245.7	0.272	5.04×10^3	1.52×10^4
	S3	172.4	0.481	1.27×10^4	3.60×10^4
1550	S1	66.1	0.547	1.73×10^4	7.38×10^4
	S2	91.4	0.400	1.30×10^4	3.73×10^4
	S3	115.7	0.680	2.08×10^4	5.78×10^4

3.2. Diffusivity

Each experiment was evaluated according to the model proposed in Ref. [11] to determine the diffusivity of magnesia. The average diffusivities of magnesia in S1–S3 at 1450, 1500, and 1550 °C are presented in Figure 4a. In a particular slag, the diffusivity of magnesia increased with increasing experimental temperature because of its lowered viscosity at higher temperatures. In addition, no trend was observed in the case of diffusivity with slag basicity; however, slag viscosities can explain the trend in diffusivities. Figure 4b shows the Arrhenius plots of the magnesia diffusivities in S1–S3 as a function of reciprocal temperature (K). The linear tendency of the Arrhenius plot confirms the plausibility of the trend in diffusivities. The activation energies of magnesia diffusion calculated from the Arrhenius plots are 213, 185, and 259 kJ/mol for S1, S2, and S3, respectively.

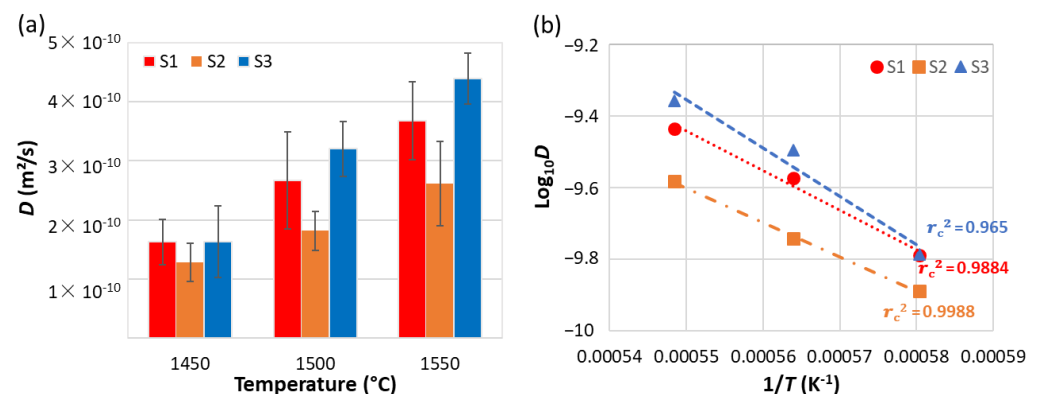
**Figure 4.** (a) Magnesia diffusivity and (b) Arrhenius plot of magnesia diffusivity in S1, S2, and S3 slags at 1450, 1500, and 1550 °C.

Table 4 shows the diffusivities of magnesia obtained from the rotating finger test and CLSM. Magnesia diffusivities determined using a rotating finger test were obtained from Ref. [8], which were determined for slag S1, as used here; however, they are not exactly valid for the virgin slag composition. In Ref. [10], the magnesia concentration of the slag increased during the experiment, which was negligible for the CLSM investigation performed in this study. Therefore, they were converted to diffusivities of the virgin slag viscosity using the Stokes–Einstein relation, where the product of the diffusivity and viscosity is constant. In addition to the diffusivity determination model (M3) proposed in Ref. [11], shrinking core models with (M2) and without (M1) Stefan flow, both exemplified in Ref. [11], were employed to determine the diffusivities from the CLSM studies. M3 showed good agreement with the rotating finger test results, where the effective boundary layer thickness could be accurately controlled. However, M1 and M2 overestimated diffusivity in all cases.

Table 4. Diffusivities of magnesia received from rotating finger test and CLSM studies.

Slag	Experimental Temperature (°C)	Diffusivities from Rotating Finger Test [8] (m ² /s)	Diffusivity from CLSM [11] (m ² /s)		
			M1	M2	M3
S1	1450	8.44781×10^{-11}	3.93×10^{-10}	2.81×10^{-10}	1.63×10^{-10}
	1500	2.04898×10^{-10}	6.48×10^{-10}	4.61×10^{-10}	2.67×10^{-10}
	1550	3.81569×10^{-10}	1.09×10^{-9}	7.71×10^{-10}	3.67×10^{-10}

4. Conclusions

HT-CLSM investigations for pore-free fragments of single-crystal fused magnesia particles in three silicate slags were carried out at 1450, 1500, and 1550 °C under an ambient atmosphere. As expected, dissolution was faster at higher temperatures because of the lower slag viscosity. In all slags, at a particular temperature, the absolute value of the dissolution rate decreased to a minimum at the beginning because of the development of a quasi-steady diffusive boundary layer, and subsequently increased because the quasi-steady diffusive boundary layer thickness decreased in accordance with the particle radius. It is often desirable to characterize dissolution trends using simple reference numbers. The results show that the dissolution trend among the slags could not be explained simply by the C/S ratio or even by B/η and $B/(\eta \cdot \delta)$. However, the introduction of a so-called thermodynamic factor and using the quotient $B \cdot f / (\eta \cdot \delta)$ greatly improve its correspondence. Therefore, the assumption of proportionality between D and f/η fits much better than that between D and $1/\eta$, although it is still imperfect. The Arrhenius plots of diffusivities show a linear trend, which confirms the plausibility of the diffusivity results, providing the opportunity to obtain the diffusivities at other temperatures without carrying out physical experiments. Furthermore, the diffusivities from the M3 model of the CLSM studies correspond well with the rotating finger test results, where the effective boundary layer thickness could be accurately controlled, increasing the reliability of the outcomes.

Author Contributions: Conceptualization, B. and H.H.; investigation—performing experiments and evaluation of results, B.; methodology, B.; formal analysis, B.; validation, B. and H.H.; writing—original draft, B.; visualization, B.; writing—review and editing, H.H.; supervision, H.H.; resources, H.H.; funding acquisition, H.H. All authors have read and agreed to the published version of the manuscript.

Funding: This research was funded by the COMET program within the K2 Center “Integrated Computational Material, Process and Product Engineering (IC-MPPE)”, project no. 859480. This program is supported by the Austrian Federal Ministries for Transport, Innovation, and Technology (BMVIT) and Digital and Economic Affairs (BMDW), represented by the Austrian Research Funding Association (FFG), and the federal states of Styria, Upper Austria, and Tyrol.

Institutional Review Board Statement: Not applicable.

Informed Consent Statement: Not applicable.

Data Availability Statement: Data supporting the findings of this study are available upon reasonable request from the corresponding author.

Acknowledgments: The authors gratefully acknowledge the helpful guidance from Volkmar Kircher regarding the experimental procedures.

Conflicts of Interest: The authors declare that they have no competing financial interests or personal relationships that may have influenced the work reported in this study.

References

- Hou, X.; Ding, D.; Xiao, G.; Jin, E.; Chong, X.; Luo, J.; Gao, Y. Corrosion Mechanism of Magnesia-Chrome Refractory Bricks with FetO-SiO₂-Cr₂O₃ Copper Converter Slag. *Ceram. Int.* **2023**, *49*, 15395–15401. [[CrossRef](#)]
- Calvo, W.A.; Pena, P.; Tomba Martinez, A.G. Post-Mortem Analysis of Alumina-Magnesia-Carbon Refractory Bricks Used in Steelmaking Ladles. *Ceram. Int.* **2019**, *45*, 185–196. [[CrossRef](#)]
- Huang, A.; Wang, Y.; Zou, Y.; Gu, H.; Fu, L. Dynamic Interaction of Refractory and Molten Steel: Corrosion Mechanism of Alumina-Magnesia Castables. *Ceram. Int.* **2018**, *44*, 14617–14624. [[CrossRef](#)]

4. Heo, J.; Park, J.H. Interfacial Reactions between Magnesia Refractory and Electric Arc Furnace (EAF) Slag with Use of Direct Reduced Iron (DRI) as Raw Material. *Ceram. Int.* **2022**, *48*, 4526–4538. [[CrossRef](#)]
5. Yu, Z.; Liu, Z.; Ye, F.; Xia, L. Corrosion Mechanism of Magnesia-Chrome and Alumina-Chrome Refractories in E-Scrap Smelting. *Ceram. Int.* **2022**, *48*, 2693–2703. [[CrossRef](#)]
6. Zou, Y.; Huang, A.; Wang, R.; Fu, L.; Gu, H.; Li, G. Slag Corrosion-Resistance Mechanism of Lightweight Magnesia-Based Refractories under a Static Magnetic Field. *Corros. Sci.* **2020**, *167*, 108517. [[CrossRef](#)]
7. Burhanuddin; Guarco, J.; Harmuth, H.; Vollmann, S. Application of an Improved Testing Device for the Study of Alumina Dissolution in Silicate Slag. *J. Eur. Ceram. Soc.* **2022**, *42*, 3652–3659. [[CrossRef](#)]
8. Burhanuddin; Harmuth, H.; Vollmann, S. Quantification of Magnesia Dissolution in Silicate Melts and Diffusivity Determination Using Rotating Finger Test. *Appl. Sci.* **2022**, *12*, 12791. [[CrossRef](#)]
9. Monaghan, B.J.; Chen, L.; Sorbe, J. Comparative Study of Oxide Inclusion Dissolution in CaO-SiO₂-Al₂O₃ Slag. *Ironmak. Steelmak.* **2005**, *32*, 258–264. [[CrossRef](#)]
10. Liu, J.; Guo, M.; Jones, P.T.; Verhaeghe, F.; Blanpain, B.; Wollants, P. In Situ Observation of the Direct and Indirect Dissolution of MgO Particles in CaO-Al₂O₃-SiO₂-Based Slags. *J. Eur. Ceram. Soc.* **2007**, *27*, 1961–1972. [[CrossRef](#)]
11. Harmuth, H. Burhanuddin Evaluation of CLSM Measurements for Dissolution Studies—A Case Study Investigating Alumina Dissolution in a Silicate Slag. *Ceram. Int.* **2022**, *48*, 28174–28180. [[CrossRef](#)]
12. Monaghan, B.J.; Nightingale, S.A.; Chen, L.; Brooks, G.A. The Dissolution Behaviour of Selected Oxides in CaO-SiO₂-Al₂O₃ Slags. *Int. Conf. Molten Slags Fluxes Salts* **2004**, *42*, 585–594.
13. Monaghan, B.J.; Chen, L. Dissolution Behavior of Alumina Micro-Particles in CaO-SiO₂-Al₂O₃ Liquid Oxide. *J. Non. Cryst. Solids* **2004**, *347*, 254–261. [[CrossRef](#)]
14. Sridhar, S.; Cramb, A.W. Kinetics of Al₂O₃ Dissolution in CaO-MgO-SiO₂-Al₂O₃ Slags: In Situ Observations and Analysis. *Metall. Mater. Trans. B* **2000**, *31*, 406–410. [[CrossRef](#)]
15. Valdez, M.; Prapakorn, K.; Cramb, A.W.; Sridhar, S. Dissolution of Alumina Particles in CaO-Al₂O₃-SiO₂-MgO Slags. *Ironmak. Steelmak.* **2002**, *29*, 47–52. [[CrossRef](#)]
16. Valdez, M.; Prapakorn, K.; Cramb, A.W.; Seetharaman, S. A Study of the Dissolution of Al₂O₃, MgO and MgAl₂O₄ Particles in a CaO-Al₂O₃-SiO₂ Slag. *Steel Res.* **2001**, *72*, 291–297. [[CrossRef](#)]
17. Liu, J.; Verhaeghe, F.; Guo, M.; Blanpain, B.; Wollants, P. In Situ Observation of the Dissolution of Spherical Alumina Particles in CaO-Al₂O₃-SiO₂ Melts. *J. Am. Ceram. Soc.* **2007**, *90*, 3818–3824. [[CrossRef](#)]
18. Liu, J.; Zhu, L.; Guo, M.; Verhaeghe, F.; Blanpain, B.; Wollants, P. In-Situ Observation of the Dissolution of ZrO₂ Oxide Particles in Mould Fluxes. *Rev. Métall.* **2008**, *105*, 255–262. [[CrossRef](#)]
19. Verhaeghe, F.; Liu, J.; Guo, M.; Arnout, S.; Blanpain, B.; Wollants, P. Determination of the Dissolution Mechanism of Al₂O₃ in CaO-Al₂O₃-SiO₂ Liquids Using a Combined Experimental-Numerical Approach. *J. Appl. Phys.* **2008**, *103*, 023506. [[CrossRef](#)]
20. Verhaeghe, F.; Liu, J.; Guo, M.; Arnout, S.; Blanpain, B.; Wollants, P. Dissolution and Diffusion Behavior of Al₂O₃ in a CaO-Al₂O₃-SiO₂ Liquid: An Experimental-Numerical Approach. *Appl. Phys. Lett.* **2007**, *91*, 124104. [[CrossRef](#)]
21. Yi, K.W.; Tse, C.; Park, J.H.; Valdez, M.; Cramb, A.W.; Sridhar, S. Determination of Dissolution Time of Al₂O₃ and MgO Inclusions in Synthetic Al₂O₃-CaO-MgO Slags. *Scand. J. Metall.* **2003**, *32*, 177–184. [[CrossRef](#)]
22. Feichtinger, S.; Michelic, S.K.; Kang, Y.B.; Bernhard, C. In Situ Observation of the Dissolution of SiO₂ Particles in CaO-Al₂O₃-SiO₂ Slags and Mathematical Analysis of Its Dissolution Pattern. *J. Am. Ceram. Soc.* **2014**, *97*, 316–325. [[CrossRef](#)]
23. Fox, A.B.; Valdez, M.E.; Gisby, J.; Atwood, R.C.; Lee, P.D.; Sridhar, S. Dissolution of ZrO₂, Al₂O₃, MgO and MgAl₂O₄ Particles in a B₂O₃ Containing Commercial Fluoride-Free Mould Slag. *ISIJ Int.* **2004**, *44*, 836–845. [[CrossRef](#)]
24. Lee, Y.; Yang, J.K.; Min, D.J.; Park, J.H. Mechanism of MgO Dissolution in MgF₂-CaF₂-MF (M=Li or Na) Melts: Kinetic Analysis via in-Situ High Temperature Confocal Scanning Laser Microscopy (HT-CSLM). *Ceram. Int.* **2019**, *45*, 20251–20257. [[CrossRef](#)]
25. Li, S.; Huang, A.; Jiang, T.; Gu, H.; Zeng, F.; Wang, X.; Zhang, S. Revealing of Rich Living Radicals in Oxide Melts via Weak Magnetic Effect on Alumina Dissolution Reaction. *J. Mol. Liq.* **2023**, *375*, 121391. [[CrossRef](#)]
26. Ogris, D.M.; Gamsjäger, E. Numerical Treatment of Oxide Particle Dissolution in Multicomponent Slags with Local Gibbs Energy Minimization. *Steel Res. Int.* **2022**, *93*, 2200056. [[CrossRef](#)]
27. Xin, J.; Gan, L.; Jiao, L.; Lai, C. Accurate Density Calculation for Molten Slags in SiO₂-Al₂O₃-CaO-MgO Systems. *ISIJ Int.* **2017**, *57*, 1340–1349. [[CrossRef](#)]
28. Bernhard, C.; Schider, S.; Sormann, A.; Xia, G.; Ilie, S. Erste Ergebnisse Des Neuen Hochtemperatur-Konfokalmikroskops Am Lehrstuhl Für Metallurgie. *BHM Berg-Hüttenmännische Monatshefte* **2011**, *156*, 161–167. [[CrossRef](#)]
29. Michelic, S.; Goriupp, J.; Feichtinger, S.; Kang, Y.-B.; Bernhard, C.; Schenk, J. Study on Oxide Inclusion Dissolution in Secondary Steelmaking Slags Using High Temperature Confocal Scanning Laser Microscopy. *Steel Res. Int.* **2016**, *87*, 57–67. [[CrossRef](#)]

Disclaimer/Publisher's Note: The statements, opinions and data contained in all publications are solely those of the individual author(s) and contributor(s) and not of MDPI and/or the editor(s). MDPI and/or the editor(s) disclaim responsibility for any injury to people or property resulting from any ideas, methods, instructions or products referred to in the content.